Applied Catalysis B: Environmental 110 (2011) 251–259

Contents lists available at SciVerse ScienceDirect

Applied Catalysis B: Environmental

journal homepage: www.elsevier.com/locate/apcatb

Highly selective one-dimensional TiO_2-based nanostructures for air treatment applications

María D. Hernández-Alonso[a,*], Sergio García-Rodríguez[b], Silvia Suárez[a], Raquel Portela[a], Benigno Sánchez[a], Juan M. Coronado[c]

[a] Environmental Applications of Solar Energy, CIEMAT-PSA, Avenida Complutense, 22, Bldg. 42, 28040 Madrid, Spain
[b] Instituto de Catálisis y Petroleoquímica, Marie Curie 2, Cantoblanco, 28049 Madrid, Spain
[c] Thermochemical Processes Unit, Instituto IMDEA Energía, Campus de la Universidad Rey Juan Carlos, C/Tulipán s/n, 28933 Móstoles, Madrid, Spain

ARTICLE INFO

Article history:
Received 27 June 2011
Received in revised form 24 August 2011
Accepted 9 September 2011
Available online 16 September 2011

Keywords:
Photocatalysis
Air treatment
Trichloroethylene
Titanate
Nanotubes
TiO_2
Hydrothermal synthesis
Photo-oxidation

ABSTRACT

The aim of the present research is to determine the optimum hydrothermal synthesis procedure for using TiO_2-based one-dimensional materials as photocatalysts for air treatment applications, in order to enhance their mineralization capacity. The prepared samples were thoroughly characterized by means of TEM, N_2 adsorption–desorption isotherms, XRD and Raman spectroscopy. Trichloroethylene (TCE) was selected as a convenient model volatile organic compound (VOC) due to its elevated reactivity. In this study, it is described how the selection of the synthesis parameters (TiO_2 precursor, hydrothermal treatment conditions, washing procedure or calcination temperature) allows modulating the nanotubes physicochemical characteristics and, thus, photoactivity. The optimization process led to nanotubes with remarkable photocatalytic performance, with high TCE conversion and selectivity to CO_2, which can be favourably compared to that of the benchmark photocatalyst Degussa P25.

© 2011 Elsevier B.V. All rights reserved.

1. Introduction

Currently, there is a significant interest in the development of methods for controlling the morphology of photocatalysts in the nanoscale, owing to the fact that nanostructured TiO_2 have shown enhanced photocatalytic performance compared to bulk titania. This improved photoactivity is attributed to the increment in surface area and the modification of the optical and electronic properties of nanosized semiconductors [1,2]. Besides, from a materials chemistry point of view, highly homogeneous photocatalysts in terms of shape, size and structure are ideal to establish correlations between physicochemical properties and activity. In this context, the discovery by Kasuga et al. [3] of a simple hydrothermal route for obtaining Ti-based nanotubular structures through the transformation of TiO_2 into titanates, with high specific surface area and narrow pore size distribution, has acquired a significant relevance. This one-dimensional morphology can lead to improved charge transport properties [4]. Moreover, the high ion-exchange capacity of the titanates can be exploited to functionalize the nanotubes, for instance with the aim of shifting the absorption edge of these materials into the visible range to use them for solar applications [5]. Another potential advantage lies in the high surface area of these materials, which is expected to increase their adsorption capacity and, therefore, favour catalytic and photocatalytic processes [4].

Although there is a growing interest in the prospective application of hydrothermally synthesized titania nanotubes as photocatalysts, research works dealing with the use of these nanostructured materials are still limited. The degradation of dyes in aqueous solutions has been usually selected as test reaction, although with not very promising results [6–12]. Leaving apart the questionable validity of using dye discoloration without TOC monitoring to establish the photocatalytic performance [13], the efficiency of titanate nanotubes was, in most cases, lower than reference TiO_2 photocatalysts. However, the elongated photocatalyst particles proved to be more easily recovered from solutions, which would be a benefit in large scale applications that could compensate, at least partly, their poorer photoactivity.

With respect to the performance of these materials for the photocatalytic degradation of pollutants in the gas phase, the results, although much more limited, are more promising. Generally, improved efficiencies under UV irradiation are reported for unmodified nanotubes, compared to those obtained with the benchmark photocatalyst Degussa P25 [14–16].

* Corresponding author.
E-mail address: mdolores.hernandez@ciemat.es (M.D. Hernández-Alonso).

0926-3373/$ – see front matter © 2011 Elsevier B.V. All rights reserved.
doi:10.1016/j.apcatb.2011.09.009

The aim of the present research is to evaluate how the different physicochemical characteristics of titanate nanotubes obtained under different preparation conditions affect their performance in the photocatalytic removal of pollutants from air streams. In a previous work [17] it was revealed that the modification of synthesis parameters makes possible the selection of the structural features of the product (e.g. aspect ratio). Now, the goal is to optimize the hydrothermal synthesis procedure for the use of these one-dimensional materials as photocatalysts for air treatment applications, in order to enhance their mineralization capacity. Although the influence of the annealing temperature on the photoactivity of the nanotubes has been previously analyzed [9,18], to the best of our knowledge, the effect of the physicochemical properties (e.g. morphology) on their performance has been scarcely taken into account [16].

Trichloroethylene (TCE) was selected as a model volatile organic compound (VOC). In the absence of water vapour in the gas stream, besides CO_2, the formation of highly toxic $COCl_2$ (phosgene) takes also place according to Eq. (1). In addition, dichloroacetyl chloride (DCAC), molecular chlorine and CO can be detected, depending on the reaction conditions [19]. However, surface hydroxyl groups may play a similar role to water in Eq. (2), providing a pathway for complete mineralization [20].

$$C_2HCl_3 + \frac{3}{2}O_2 \rightarrow COCl_2 + HCl + CO_2 \quad (1)$$

$$C_2HCl_3 + \frac{3}{2}O_2 + H_2O \rightarrow 3HCl + 2CO_2 \quad (2)$$

Thus, TCE is a suitable molecule to study the influence of synthetic parameters on the selectivity of the materials. According to this, finding a photocatalyst that can provide a high selectivity to CO_2 during the photo-oxidation of TCE in the absence of water, combined with a competitive conversion, is crucial for efficient air detoxification.

2. Experimental

2.1. Synthesis of titanate nanotubes

The Ti-based nanostructures were obtained from different TiO_2 precursors and under different hydrothermal synthesis conditions, as summarized in Table 1. TiO_2/NaOH ratio (14 g/L) and NaOH concentration (10 M) were maintained constant in all cases.

In a first step of the procedure, 1 g of the precursor (anatase/rutile, 21 nm (Degussa P25); anatase, 10 nm (Hombikat UV-100); anatase, 78 nm (BDH); rutile, 63 nm) was hydrothermally treated at 130–150 °C in 70 mL of 10 M NaOH in a Teflon-lined autoclave, for a period of time between 24 and 72 h. The mixture was stirred for 30 min before and after the thermal treatment. In a second stage, the obtained powders were thoroughly washed using different washing agents (i.e. HCl, HNO_3 or H_2O). The powders were recovered from the solutions by centrifugation, with the exception of the sample labeled as TNT6-HCl-d, which was recovered by decantation. In every case, the products were dried at 100 °C overnight. Some selected samples were calcined for 3 h at different temperatures in the range 250–500 °C.

Samples are labeled as TNT*x*, where *x* defines the precursor and the hydrothermal conditions, followed by the washing agent. The name of calcined samples includes the calcination temperature.

2.2. Textural and structural characterization

BET surface area and average pore diameter values were estimated from N_2 adsorption isotherms, measured at 77 K in a Micromeritics 2100 automatic apparatus. Powder XRD patterns were recorded on a Seifert XRD 3000P diffractometer using Ni-filtered Cu K_α radiation in the Bragg–Brentano geometry. The samples were also characterized by *in situ* variable temperature X-ray powder diffraction (XRD) with a Philips PW 3040/00 X'Pert MPD/MRD diffractometer at a scanning rate of $0.2^\circ\ s^{-1}$. A JEM-2100F 200 kV transmission electron microscope (JEOL Ltd.), equipped with an Oxford INCAx-Sight Energy Dispersive X-Ray Spectroscopy (EDS) detector (Oxford Instruments Ltd.), was used to study the crystallinity, chemical composition and morphology of the samples.

A spectroscopic characterization of the samples was also performed. Laser Raman spectra were obtained with a Renishaw Micro-Raman System 1000 equipped with a cooled CCD detector and a holographic super-Notch filter that removes the elastic scattering. The samples were excited at 488 nm.

2.3. Photocatalytic activity measurements

The photocatalytic oxidation of gas-phase trichloroethylene, selected as a model VOC molecule, was studied in a continuous plug flow flat photoreactor. This photoreactor, with external dimensions 120 mm × 50 mm × 10 mm (length × wide × depth), was constructed in stainless steel except for one window of 27 cm^2, closed with a borosilicate glass with low iron content. The powdered samples, after dispersion in 2-propanol, were coated on a microscope slide located under the glass window. Irradiation was provided by two UVA Philips TL-8W/05 fluorescent lamps with maximum emission at 365 nm wavelength, resulting in sample irradiance of 4.4 mW/cm^2. A gas mixture of TCE and air was prepared using a gas cylinder of TCE/N_2 (Air Liquide, 250 ppm) and compressed air free of water and CO_2. Flow rate, pressure, temperature, UV radiation and relative humidity were controlled by an automated equipment using electronic mass flow controllers and automated valves. TCE concentration was fixed at 30 ppm, and total gas flow varied between 100 and 300 ml/min (residence time = 1.98–0.66 s). The gas-phase composition was continuously monitored using a FTIR Thermo-Nicolet 5700 spectrometer, provided with a temperature controlled multiple-reflection gas cell (optical path 2 m) maintained at 110 °C. IR spectra were registered after accumulation of 64 scans at a resolution of 4 cm^{-1}. TCE and reaction products evolution, obtained by integrating the area under the characteristic IR band for each component, was monitored on-line. Selectivity to CO_2 was estimated according to the carbon balance (Eq. (3))

$$S_{CO_2} = \frac{CO_2}{2 \times (TCE_{inlet} - TCE_{outlet})} \times 100 \quad (3)$$

3. Results

A summary of the synthesis parameters and the textural properties of the materials is presented in Table 1. TCE photocatalytic degradation results obtained with the different samples are shown in Table 2. The values of steady-state conversion and selectivity to CO_2 at the three different flow rates assayed are presented. A detailed description of the effect of synthetic parameters on the photocatalytic performance of the obtained one-dimensional nanostructures is given as follows.

3.1. Influence of the washing procedure

As a general procedure, the powders recovered by centrifugation after the hydrothermal treatment were subjected to an acidic washing process, either in HCl or HNO_3. In order to analyze the influence that this washing stage exerts on the morphology and

Table 1
Synthesis and post-synthesis parameters of photocatalysts and specific surface area and pore volume values estimated by the BET method.

Sample	TiO_2 precursor	HT conditions	S_{BET} (m^2/g)	Pore volume (cm^3/g)
Degussa P25	–	–	48	0.25
TNT1-HCl	Degussa P25 (A/R) 21 nm	T = 130 °C, t = 24 h	n.m.	n.m.
TNT1-HNO_3			241	0.29
TNT2-0		T = 130 °C, t = 48 h	n.m.	n.m.
TNT2-H_2O			154	0.18
TNT2-HNO_3			390	1.28
TNT2-HCl			397	1.15
TNT2-HCl-250 °C			n.m.	n.m.
TNT2-HCl-300 °C			354	1.22
TNT2-HCl-350 °C			n.m.	n.m.
TNT2-HCl-400 °C			221	1.02
TNT2-HCl-450 °C			n.m.	n.m.
TNT2-HCl-500 °C			126	0.80
TNT3-HNO_3		T = 130 °C, t = 72 h	419	1.38
TNT3-HNO_3-300 °C			356	1.37
TNT3-HNO_3-350 °C			n.m.	n.m.
TNT3-HCl			413	1.43
TNT4-HNO_3		T = 150 °C t = 48 h	395	1.35
TNT5-HNO_3	Hombikat (A), 10 nm	T = 130 °C, t = 48 h	426	0.80
TNT5-HNO_3-300 °C			n.m.	n.m.
TNT5-HCl			n.m.	n.m.
TNT6-0	BDH (A), 78 nm	T = 130 °C, t = 48 h	57	0.16
TNT6-H_2O			197	0.68
TNT6-HNO_3			326	0.85
TNT6-HCl-d*			342	1.14
TNT7-HNO_3	Rutile (R), 63 nm	T = 130 °C, t = 48 h	251	0.77
TNT8-HNO_3		T = 150 °C, t = 48 h	293	0.74

n.m., not measured.
*In this case, decantation was used as separation method instead of centrifugation.

photocatalytic activity of the nanotubes, additional samples without any washing treatment (TNT*x*-0) or washed merely with water (TNT*x*-H_2O) were also prepared.

Fig. 1 contains the TEM micrographs of the materials obtained from TiO_2 Degussa P25 after undergoing different washing procedures. Non-nanotubular morphologies were found in TNT2-0, directly dried after recovery, consisting in globular agglomerates enriched in Na (>40% at.), as estimated by EDS analysis. Similar results were observed for the analogous samples TNT3-0 and TN4-0. The samples washed with distilled water still contained a significant amount of Na (>10% at.). As TEM micrographs and EDS analysis evidenced, a thorough washing with an acid solution (HNO_3 or HCl) is required in order to guarantee the desired nanotubular morphology and to completely remove the alkaline cations from the titanates. BET surface area remarkably increases after acidic washing. A detailed description of the influence of the

Table 2
Trichloroethylene conversions and selectivities to CO_2 obtained during the photocatalytic oxidation of the organic compound in air at 100, 200, and 300 ml/min.

Sample	TiO_2 precursor	TCE conversion, % (selectivity to CO_2, %)		
		100 ml/min	200 ml/min	300 ml/min
Degussa P25	–	100 (60)	93 (54)	81 (51)
TNT1-HCl	Degussa P25 (A/R) 21 nm	98 (62)	87 (53)	73 (52)
TNT1-HNO_3		n.m.	n.m.	n.m.
TNT2-0		12 (50)	0 (–)	0 (–)
TNT2-H_2O		11 (92)	1 (–)	1 (–)
TNT2-HNO_3		68 (60)	36 (65)	24 (68)
TNT2-HCl		82 (69)	49 (71)	34 (71)
TNT2-HCl-250 °C		96 (64)	79 (61)	62 (61)
TNT2-HCl-300 °C		100 (67)	91 (60)	81 (60)
TNT2-HCl-350 °C		100 (69)	92 (60)	81 (57)
TNT2-HCl-400 °C		100 (61)	94 (54)	83 (53)
TNT2-HCl-450 °C		100 (66)	95 (58)	85 (57)
TNT2-HCl-500 °C		100 (65)	94 (56)	83 (52)
TNT3-HNO_3		64 (64)	34 (66)	22 (71)
TNT3-HNO_3-300 °C		96 (66)	80 (61)	64 (57)
TNT3-HNO_3-350 °C		100 (76)	95 (64)	89 (62)
TNT3-HCl		71 (66)	40 (64)	26 (67)
TNT4-HNO_3		70 (67)	40 (66)	27 (67)
TNT5-HNO_3	Hombikat (A), 10 nm	79 (65)	43 (68)	29 (67)
TNT5-HNO_3-300 °C		97 (67)	86 (58)	70 (60)
TNT5-HCl		67 (69)	46 (42)	25 (61)
TNT6-0	BDH (A), 78 nm	n.m.	n.m.	n.m.
TNT6-H_2O		19 (90)	2 (100)	0 (0)
TNT6-HNO_3		59 (58)	25 (71)	17 (68)
TNT6-HCl-d		48 (81)	24 (83)	15 (89)
TNT7-HNO_3	Rutile (R), 63 nm	38 (66)	19 (73)	13 (76)
TNT8-HNO_3		62 (65)	34 (64)	22 (65)

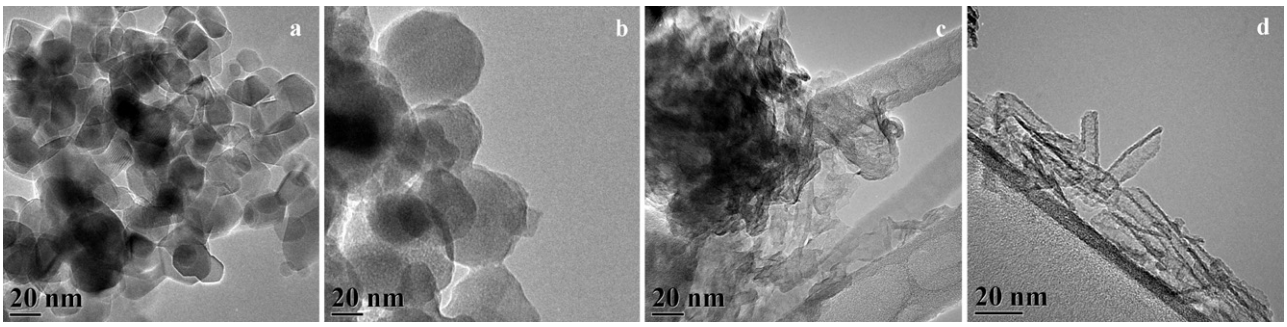

Fig. 1. Influence of the washing procedure on the morphology of the TNT2 samples: (a) Degussa P25 used as TiO_2 precursor; (b) before washing (TNT2-0); (c) after washing with H_2O (TNT2-H_2O); (d) after washing with HNO_3 (TNT2-HNO_3).

washing stage on the morphology of the nanotubes can be found elsewhere [17].

As it can be clearly observed in Fig. 2, the notable Na^+ content in TNT2-0 and TNT2-H_2O resulted in an inhibited performance of the titanates in the photocatalytic oxidation of TCE, as it could be expected [14]. In this particular photocatalytic reaction, the slightly higher conversion yielded by the sample washed with HCl, compared with the one washed with HNO_3, could be ascribed to the presence of residual Cl^- ions on this material (not detected in the EDS analysis), that might contribute to the chain reaction of the chlorine radicals usually found in TCE photodegradation [21]. However, it must be taken into account that chlorine can also act poisoning the catalyst surface [22] and, consequently, other unnoticed factors could be contributing to the higher activity of TNT2-HCl sample. In fact, although washing with HCl gave also better results for TNT3 sample, the contrary was observed for TNT5.

3.2. Influence of the hydrothermal treatment conditions

The influence of time and temperature of the hydrothermal treatment applied to the TiO_2 source was studied using TiO_2 Degussa P25 as precursor.

XRD patterns indicated the formation of a protonated layered titanate after acidic washing, either in HNO_3 or HCl. The XRD patterns showed that crystallinity tends to increase when harsher hydrothermal conditions are used, as indicated by the growing intensity of the diffraction peaks (Fig. 3). This tendency is accompanied by a moderate decrease in the interlayer spacing of the nanotubes walls, from 9.2 to 8.0 Å, as estimated also from the XRD patterns [17].

However, the morphological analysis of the materials concluded that a 24 h treatment (TNT1) was not sufficient for the complete precursor transformation into titanate nanotubes. Branched nanostructures (Fig. 4a) or mixtures of poorly defined nanotubes and aggregates of globular shape were observed instead. On the other hand, longer treatments (TNT2 and TNT3) yielded nanotubular structures as the only product (Fig. 4b). Apart from a slight increase in both the diameter and the length of the tubes, nanostructures obtained at 48 h or 72 h looked fairly similar. The temperature increase up to 150 °C (TNT4) led also to morphologies akin to TNT3. The estimated specific surface area (S_{BET}), presented in Table 1, did not experience any significant change either.

Fig. 5 represents the effect of the hydrothermal synthesis conditions on the photoactivity of the catalysts washed in acidic conditions. The highest conversion was achieved with the branched material TNT1 (24 h, 130 °C) in the whole range of flow rates. A significant lower performance was exhibited by TNT2 (48 h, 130 °C) photocatalyst, while TNT3 and TNT4 (the last one not shown in the graph for the sake of clarity), prepared under harsher conditions, showed the lowest TCE conversion. These results may lead to consider that high crystallinity, together with longer dimensions of the nanotubes, cause a detrimental effect on the photocatalytic performance of these one-dimensional nanostructures. However, it is worth noting that TNT2 yielded the highest selectivity to CO_2, significantly higher than TNT1, which was translated in lower production of phosgene and other by-products. For a similar TCE conversion value (82–87%), TNT2-HCl provided a 16% higher selectivity to CO_2 than TNT1-HCl (Table 2). Furthermore, the selectivity to CO_2 did not experience any detriment for TNT2 or TNT3 when

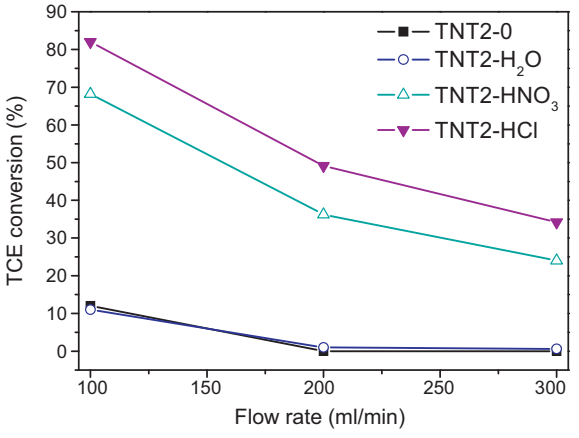

Fig. 2. Influence of the washing procedure on the photocatalytic activity of sample TNT2 in the degradation of TCE.

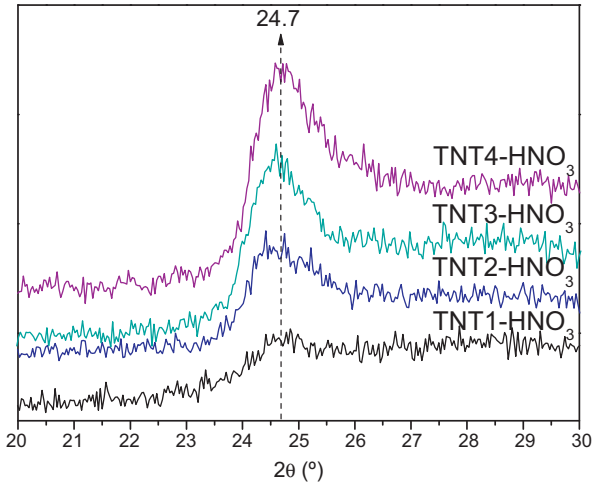

Fig. 3. Detail of the diffraction peak at ca. 24.7° from the titanate phase of samples TNT1, TNT2, TNT3, and TNT4 after acidic washing with HNO_3.

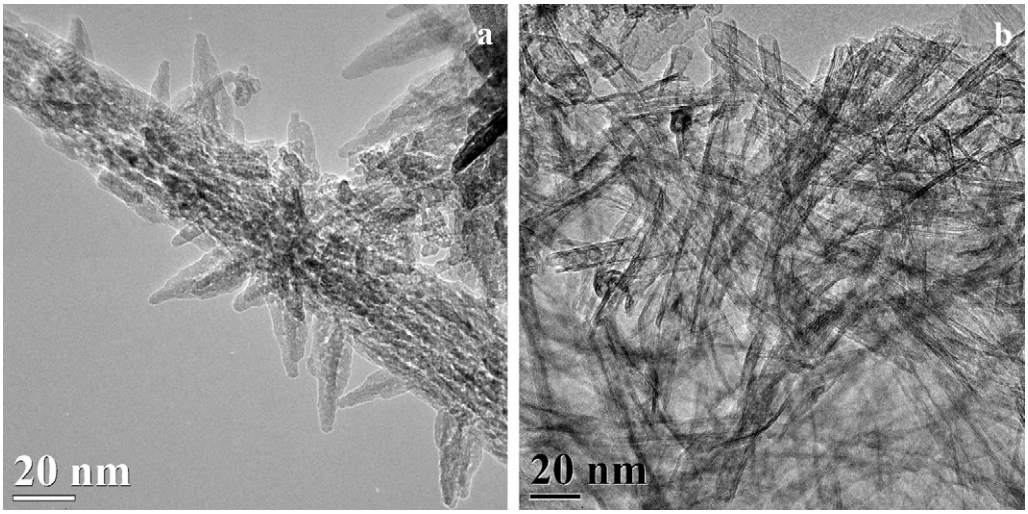

Fig. 4. TEM micrographs of nanostructures obtained, after acidic washing with HCl, from commercial Degussa P25 TiO_2 treated at 130 °C for: (a) 24 h (TNT1-HCl) and (b) 72 h (TNT3-HCl).

increasing the flow rate, in contrast to the behaviour observed with TNT1. These results seem to indicate that the direct reaction pathway described by Eq. (2) is favoured when using these samples. On the other hand, no nanotubular morphologies were detected in TNT1. Thus, despite the evident potential of TNT1 as photocatalyst, the conditions applied to obtain TNT2 nanotubes were settled as the standard procedure.

3.3. *Influence of the TiO_2 precursor*

Once it was proved that the hydrothermal treatment in NaOH 10 M of Degussa P25 for 48 h at 130 °C was appropriate to produce photocatalytically active titanate nanotubes, an analogous treatment was applied to different samples of commercially available TiO_2 nanoparticles. Titania with different crystalline phases and/or sizes were selected as precursors (TNT5 to TNT7, Table 1). An additional sample from rutile, named TNT8, was synthesized increasing the hydrothermal treatment temperature up to 150 °C, in order to assure the complete transformation of this phase, more stable than anatase. Some unreacted rutile was detected in the XRD pattern of TNT7 sample, obtained at 130 °C, which disappeared at 150 °C (TNT8) (Fig. 6).

TEM micrographs showing the morphology of the products obtained from the different titania after the acidic washing stage are shown in Fig. 7. As thoroughly described in a previous work [17], rutile-TiO_2 gave rise to long and well-formed nanotubes. Anatase-TiO_2 of similar crystal size (TiO_2 BDH) also produced quite regular nanotubes, although significantly shorter. On the other hand, the nanotubular structures obtained from anatase/rutile mixtures (Degussa P25) or pure anatase with smaller crystal size (Hombikat UV-100) rendered irregular and poorly defined tubular structures. Their lower aspect ratio and heterogeneity, accompanied by lower crystallinity (see Fig. 6, inset), were also translated into significantly higher surface area.

As observed for samples treated at different hydrothermal conditions, the lower crystallinity in TNT2 and TNT5 was accompanied by a longer interlayer spacing of the nanotubes walls (8.9 and 8.5 Å respectively) compared to, for example, TNT8 (7.7 Å) [17]. These structural and morphological characteristics seem to be responsible for the better performance achieved when TNT2 or TNT5 were used as photocatalysts. As it can be observed in Fig. 8, TNT5 presents higher TCE conversion in the whole range of flow rates than TNT6 and TNT8. On the other hand, selectivities to CO_2 are similar and

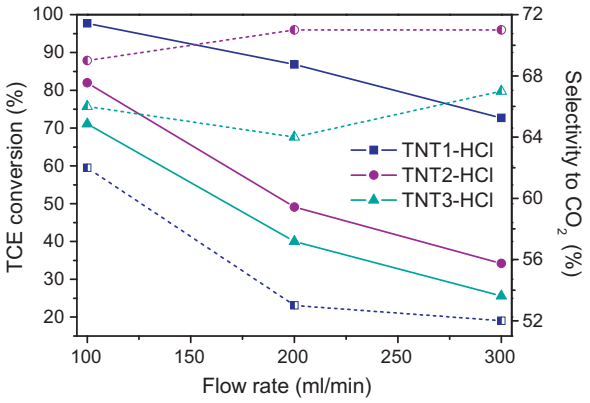

Fig. 5. Effect of the hydrothermal treatment conditions on the photocatalytic degradation of TCE. Conversion is represented by solid lines, while selectivity to CO_2 is represented by dashed lines.

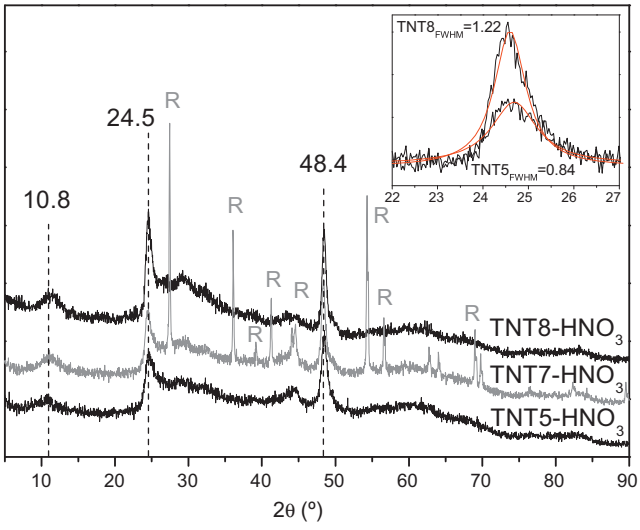

Fig. 6. XRD patterns of samples TNT5-HNO_3, synthesized from anatase (TiO_2 Hombikat), and TNT7-HNO_3 and TNT8-HNO_3, synthesized from rutile. The inset contains a detail of the diffraction peak at 24.5°, from the titanate phase, with the estimated FWHM values.

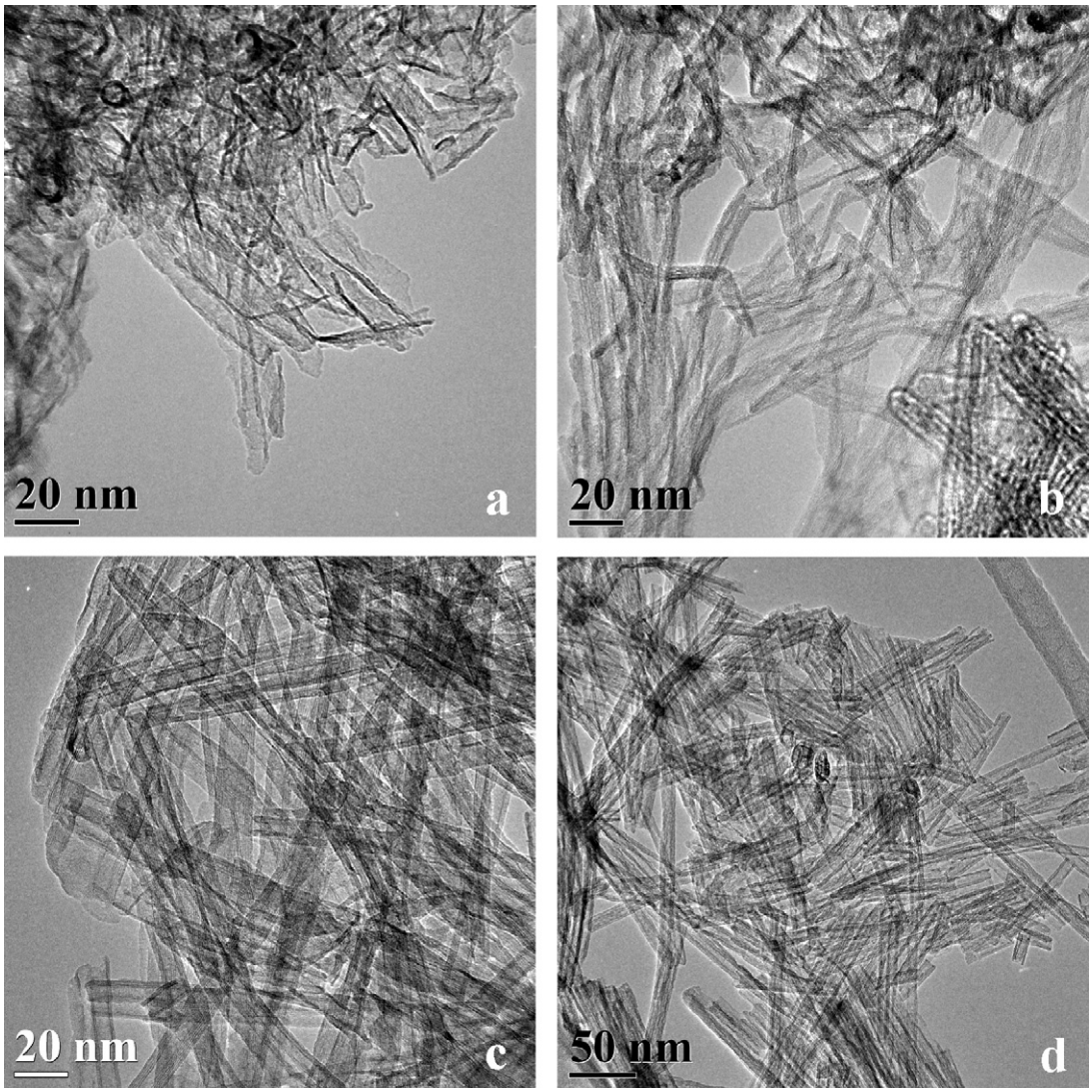

Fig. 7. TEM images of HNO_3-washed samples obtained from different TiO_2 sources: (a) anatase/rutile, 21 nm (TNT2-HNO_3); (b) anatase, 10 nm (TNT5-HNO_3); (c) anatase, 78 nm (TNT6-HNO_3) and (d) rutile, 63 nm (TNT8-HNO_3).

around 60–70%, as can be found in Table 2. Irregular nanotubular structures with low aspect ratios (length/width), shoddily defined, demonstrated higher photocatalytic activity than long, high crystalline, well-defined nanotubes. In fact, there seems to be a direct correlation between the surface area of the protonated titanate nanotubes and the photoactivity, as shown in Fig. 9. It is also worth remarking that the presence of unreacted rutile phase in sample TNT7 resulted in a considerable detriment of photoactivity compared to that of TNT8.

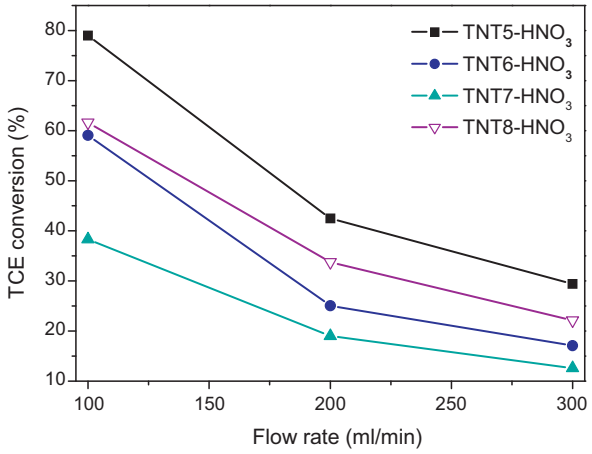

Fig. 8. Effect of the TiO_2 precursor on the photocatalytic activity.

3.4. Influence of the calcination temperature

It is worth emphasizing that all samples described above were not subjected to any post-synthesis thermal treatment, apart from a drying stage at 100 °C. Thus, after evaluating the effect of the different synthetic parameters in the nanotube formation and photocatalytic performance, the search for the optimum calcination temperature was carried out. The *in situ* temperature-controlled XRD patterns of sample TNT2-HCl are plotted in Fig. 10a. A progressive transformation of the titanate structure into anatase, from room temperature up to 400–450 °C, was evidenced by the shift of the corresponding diffraction peaks, together with the changes in their relative intensity. From that point on, the temperature rise led to an increase in the intensity and sharpening of the anatase diffraction peaks, which can be read as a crystal size growth. The temperature threshold of the phase transformation, from titanate to anatase, is more clearly visualized in Fig. 10b. When the samples

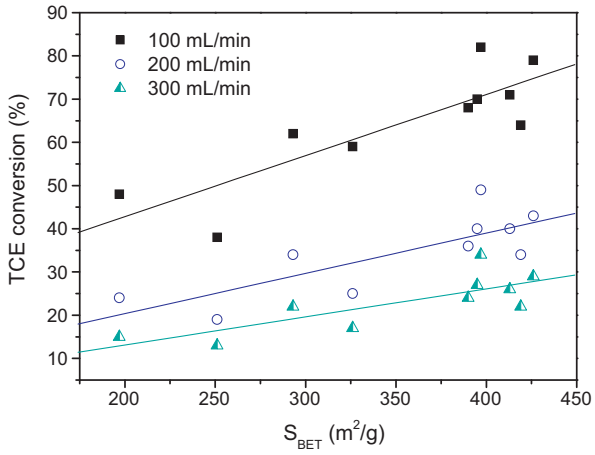

Fig. 9. Correlation between the surface area of the protonated titanate nanotubes and their photoactivity.

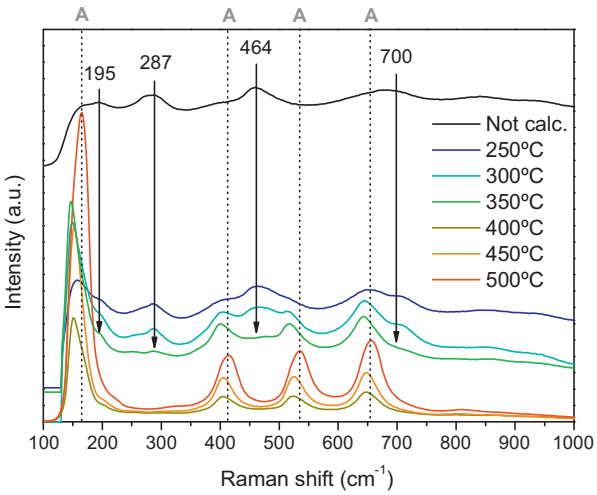

Fig. 11. Raman spectra of sample TNT2-HCl after calcination at different temperatures. A indicates the anatase vibrational modes.

were calcined for 3 h, the previously described transition shifted to a lower temperature, as the Raman spectra show in Fig. 11. Thus, at 350 °C the H-titanate bands, being the most representative ones at around 195, 287, 464 and 700 cm^{-1}, coexist with the emerging bands of anatase. TEM micrographs (Fig. 12) indicate that the nanotubular morphology is still predominant at this temperature (350 °C), although the structures have been clearly affected and some other morphologies are now observed, including fragments of nanotubes. After calcination at 400 °C, the Raman vibrational modes assigned to the anatase phase dominate the spectrum, while the modes corresponding to the H-titanate cannot be distinguished. At 500 °C, titanate nanotubes have evolved into elongated anatase particles (Fig. 12c). As expected, the values of BET surface area decreased as calcination temperature was increased, from the initial 397 m^2/g of TNT2-HCl to 127 m^2/g of the sample calcined at 500 °C. It is worth remarking that the A_{1g} mode of the anatase structure, generally detected at 144 cm^{-1}, appears at a higher frequency in the case of the anatase derived from the nanotubular structure. Similar results were obtained by *in situ* thermo-Raman by Cortés-Jácome et al. [23], who observed the beginning of the transformation of the nanotubes into anatase at around 400 °C. They attributed the shift in the A_{1g} mode to the formation of a non-stoichiometric TiO_2-*x* during the hydroxylation of the nanotubes.

The effect of the calcination temperature on the photocatalytic activity of these materials is plotted in Fig. 13, where both the TCE conversion and the selectivity to CO_2 exhibited by the synthesized photocatalysts are presented. On one hand, a considerable enhancement of TCE conversion was obtained increasing the calcination temperature up to 300 °C, reaching the values obtained with the benchmark photocatalyst Degussa P25. From 300 °C to 500 °C, the improvement in the photocatalysts performance was marginal, only observed at high flow rates for samples calcined at 450 and 500 °C. On the other hand, higher selectivity to CO_2 was achieved with titania nanotubes than with Degussa P25, being this improvement especially significant for samples calcined at 300–350 °C. Thus, the maximum conversion and selectivity to CO_2 in the photocatalytic degradation of TCE in gas phase were achieved with nanotubes annealed at these temperatures (Table 2). These samples maintain the nanotubular morphology after calcination and improve the performance of the reference photocatalyst (Degussa P25). Photoactivity dependence on the annealing temperature of nanotubes has been previously observed with similar results [9,24]. Despite the larger surface area of the non-calcined or low-temperature calcined materials, optimum values of TCE

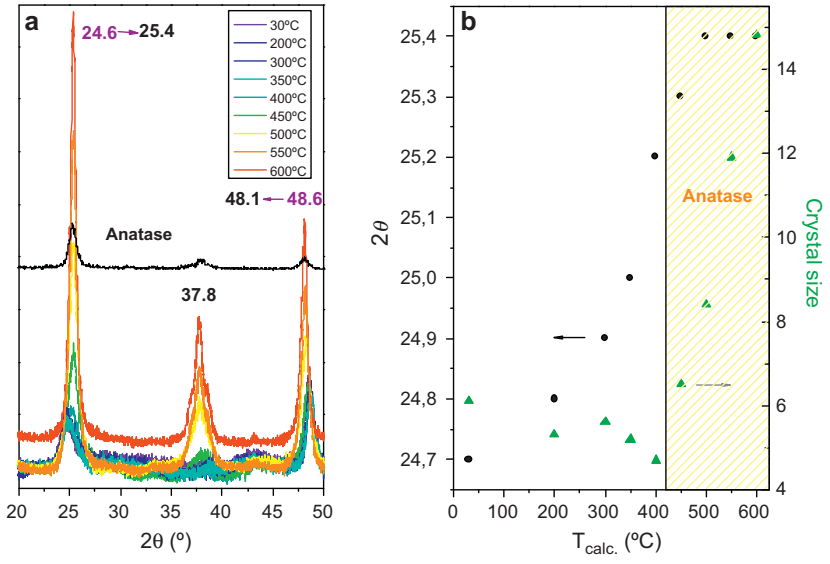

Fig. 10. (a) *In situ* temperature-controlled XRD patterns of sample TNT2-HCl and (b) effect of temperature on the diffraction peak position (at ca. 24–25°) and crystal size.

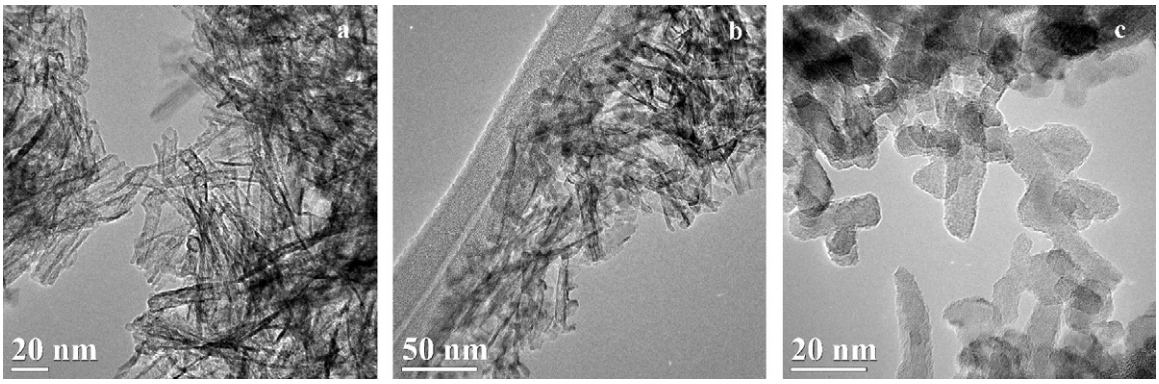

Fig. 12. TEM images of sample TNT2-HCl after calcination at: (a) 250 °C; (b) 350 °C; (c) 500 °C.

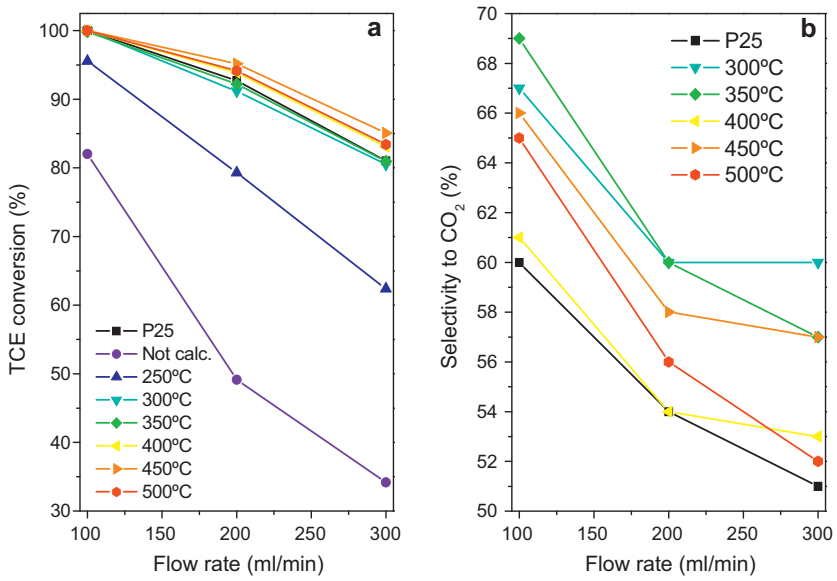

Fig. 13. Effect of calcination temperature on the photocatalytic activity of sample TNT2-HCl and comparison with the TiO_2 precursor (Degussa P25): (a) TCE conversion; (b) selectivity to CO_2.

conversion were only achieved with samples treated at $T \geq 300$ °C. The reason for this improvement can be tentatively attributed to a higher crystallinity and/or to the growing presence of TiO_2 in the annealed nanostructures. Indeed, although the titanate structure still predominated in the samples annealed at 300–350 °C, there was a progressive transformation of the structure into anatase with temperature, as revealed by the shift to higher angles of the peak at around 24–25° (Fig. 10b), from the position of the (1 1 0) plane of the protonated titanate to the (1 0 1) of anatase. These changes imply a densification of the structure as the spacing of the different planes decreases, and this fact may influence the electronic transport in the solid. Other authors have previously proposed that, during calcination, there is a gradual collapse of the structural layers of the nanotubes that results in the formation of anatase domains on their walls [23,25]. Such structural variation correlates well with the increment of photoactivity, as represented in Fig. 14, and suggests a modification of the electronic properties, which can be associated to the incipient formation of anatase. On the other hand, it is worth mentioning that no significant differences were observed in the TCE conversion obtained with the photocatalysts treated at 300–350 °C and the one calcined at 500 °C, which contained only TiO_2 anatase nanocrystals, or the commercial Degussa P25 (anatase/rutile TiO_2).

In any case, the samples treated at 300–350 °C presented the best mineralization yields due to the optimal balance between surface and structural properties. The reasons for the high selectivity to CO_2 of these catalysts probably lies on the surface characteristics of the nanotubes, e.g. the different OH groups population or surface acidity, as it has been reported that titanate nanotubes contain both Brønsted and Lewis acid sites, being able to behave as highly active acid catalysts [14,26]. Other studies claim that the

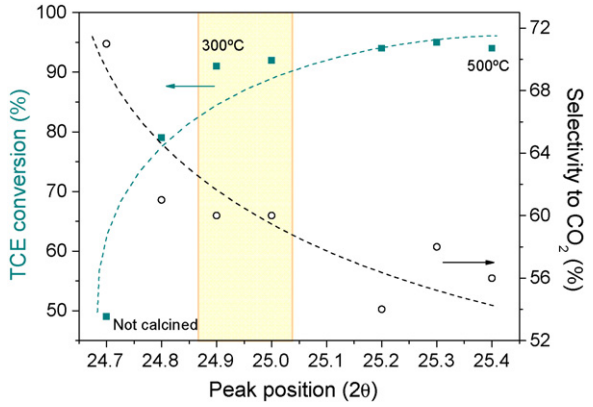

Fig. 14. Correlation between photoactivity (TCE conversion and selectivity to CO_2 at 200 ml/min) and the progressive shift of the diffraction peak from the position of the (1 1 0) plane of the protonated titanate to the (1 0 1) of anatase with calcination temperature.

number of accessible Ti–OH groups in nanotubes is higher than that in nanoparticles due to the particular topography of the nanotubular structure. These surface OH groups have been reported as highly reactive [27].

In order to gain a better understanding of the different photocatalytic behaviour of nanotubes with respect to TiO_2 nanocrystals, *operando* analysis of the catalysts surface during the photocatalytic reaction will be approached in future works.

4. Conclusions

In this research, it has been evaluated how the characteristics of titanate nanotubes obtained under different preparation conditions affect their performance in the photocatalytic treatment of air streams.

Protonated titanate nanotubes have proved to be remarkably more photoactive than the Na-titanate materials obtained before the acidic washing. For photocatalytic purposes, Na^+ must be completely removed and exchanged by protons.

The selection of the synthesis parameters allows modulating the crystallinity, textural properties and morphology of the nanotubes and, thus, their photoactivity. It was observed, for example, that irregular and shoddily defined nanotubes of high aspect ratio demonstrated higher photocatalytic activity than long, high crystalline, well-defined nanotubes. This fact seems to be connected with the larger surface area of these protonated titanate nanostructures.

Increasing the temperature of the post-synthesis thermal treatment to $T \geq 300\,^{\circ}C$ boosted the photocatalytic activity of these materials. At $T = 300$–$350\,^{\circ}C$, the highest conversion and selectivity to CO_2 was achieved in the photo-oxidation of TCE while maintaining the nanotubular morphology. This increment in TCE conversion correlates well with the progressive transformation of the structure into anatase TiO_2 with temperature. Increasing calcination temperature above this point ($T > 350\,^{\circ}C$), which led to the complete transformation of the titanate nanotubes into anatase elongated particles, did not produce an improvement in the photocatalytic activity. The performance of calcined nanotubes can be favourably compared to that of the benchmark photocatalyst Degussa P25 since it was observed that the nanotubular morphology promotes the reaction pathway that facilitates the hydrolysis of phosgene and, consequently, increases the selectivity to CO_2 during TCE photo-oxidation.

Acknowledgments

Financial support from the Spanish Ministry of Science and Innovation (MICINN, MAT2008-01094/MAT) is greatly appreciated. M.D.H. and S.S. also thank MICINN for the award of their postdoctoral contracts. The authors would like to thank V. de la Peña-O'Shea for the *In Situ* Temperature Controlled XRD measurement and G. Ledesma Pedraz for his contribution to this work.

References

[1] S. Monticone, R. Tufeu, A.V. Kanaev, E. Scolan, C. Sanchez, Appl. Surf. Sci. 162–163 (2000) 565–570.
[2] M. Fernández-García, A. Martínez-Arias, J.C. Hanson, J.A. Rodríguez, Chem. Rev. 104 (2004) 4063.
[3] T. Kasuga, M. Hiramatsu, A. Hoson, T. Sekino, K. Niihara, Langmuir 14 (1998) 3160–3163.
[4] D.V. Bavykin, F.C. Walsh, Eur. J. Inorg. Chem. (2009) 977–997.
[5] X.M. Sun, Y.D. Li, Chem. Eur. J. 9 (2003) 2229–2238.
[6] H.Y. Zhu, Y. Lan, X.P. Gao, S.P. Ringer, Z.F. Zheng, D.Y. Song, J.C. Zhao, J. Am. Chem. Soc. 127 (2005) 6730–6736.
[7] H.G. Yu, J.G. Yu, B. Cheng, J. Lin, J. Hazard. Mater. 147 (2007) 581–587.
[8] J.H. Jang, K.-S. Jeon, S. Oh, H.-J. Kim, T. Asahi, H. Masuhara, M. Yoon, Chem. Mater. 19 (2007) 1984–1991.
[9] M. Qamar, C.R. Yoon, H.J. Oh, N.H. Lee, K. Park, D.H. Kim, K.S. Lee, W.J. Lee, S.J. Kim, Catal. Today 131 (2008) 3–14.
[10] K.S. Lin, C.C. Lo, N.B. Chang, Nano 3 (2008) 257–262.
[11] L.L. Costa, A.G.S. Prado, J. Photochem. Photobiol. A Chem. 201 (2009) 45–49.
[12] B.C. Viana, O.P. Ferreira, A.G. Souza, C.M. Rodrigues, S.G. Moraes, J. Mendes, O.L. Alves, J. Phys. Chem. C 113 (2009) 20234–20239.
[13] J.M. Herrmann, Appl. Catal. B 99 (2010) 461–468.
[14] M.A. Khan, H.T. Jung, O.B. Yang, J. Phys. Chem. B 110 (2006) 6626–6630.
[15] J.A. Grasser, D.S. Muggli, Rev. Sci. Instrum. 80 (2009) 075106.
[16] S. Chatterjee, K. Bhattacharyya, P. Ayyub, A.K. Tyagi, J. Phys. Chem. C 114 (2010) 9424–9430.
[17] M.D. Hernández-Alonso, S. García-Rodríguez, B. Sánchez, J.M. Coronado, Nanoscale 3 (2011) 2233–2240.
[18] S. Wadhwa, J.J. Hamilton, P.S.M. Dunlop, C. Dickinson, J.A. Byrne, J. Adv. Oxid. Technol. 14 (2011) 147–157.
[19] W.A. Jacoby, M.R. Nimlos, D.M. Blake, R.D. Noble, C.A. Koval, Environ. Sci. Technol. 28 (1994) 1661–1668.
[20] S. Suárez, J.M. Coronado, R. Portela, J.C. Martín, M. Yates, P. Ávila, B. Sánchez, Environ. Sci. Technol. 42 (2008) 5892–5896.
[21] M.R. Nimlos, W.A. Jacoby, D.M. Blake, T.A. Milne, Environ. Sci. Technol. 27 (1993) 732–740.
[22] S.-K. Joung, T. Amemiya, M. Murabayashi, K. Itoh, J. Photochem. Photobiol. A Chem. 184 (2006) 273–281.
[23] M.A. Cortés-Jácome, G. Ferrat-Torres, L.F. Flores Ortiz, C. Ángeles-Chávez, E. López-Salinas, J. Escobar, M.L. Mosqueira, J.A. Toledo-Antonio, Catal. Today 126 (2007) 248–255.
[24] J.A. Toledo-Antonio, M.A. Cortés-Jácome, S.L. Orozco-Cerros, E. Montiel-Palacios, R. Suarez-Parra, C. Angeles-Chavez, J. Navarete, E. Lopez-Salinas, Appl. Catal. B Environ. 101 (2010) 747.
[25] J.A. Toledo-Antonio, S. Capula, M.A. Cortés-Jácome, C. Angeles-Chávez, E. López-Salinas, G. Ferrat, J. Navarrete, J. Escobar, J. Phys. Chem. C 111 (2007) 10799–10805.
[26] M. Kitano, K. Nakajima, J.N. Kondo, S. Hayashi, M. Hara, J. Am. Chem. Soc. 132 (2010) 6622–6623.
[27] A. Rendón-Rivera, J.A. Toledo-Antonio, M.A. Cortés-Jácome, C. Angeles-Chávez, Catal. Today 166 (2011) 18–24.